

**THIN METAL FILM PHYSICAL
VAPOR DEPOSITION SYSTEM**

By

Matthew D. Bowman

A thesis submitted in partial fulfillment of the
requirements for the degree of

Bachelor of Science

Houghton University

May 2023

Signature of Author.....

Department of Physics
May 10, 2023

.....

Dr. Brandon Hoffman
Professor of Physics
Research Supervisor

.....

Dr. Mark Yuly
Professor of Physics

THIN METAL FILM PHYSICAL VAPOR DEPOSITION SYSTEM

By

Matthew D. Bowman

Submitted to the Department of Physics
on May 10, 2023 in partial fulfillment of the
requirement for the degree of
Bachelor of Science

Abstract

A low-cost, thin film deposition system utilizing physical vapor deposition is being constructed at Houghton University. A mechanical pump and turbomolecular pump lower the chamber to a base pressure of 10^{-6} Torr. Three graphite crucibles are heated via thermionic emission from three corresponding tungsten filaments. Each filament floats at up to -4 kV with individually controlled currents of up to 3 A. The use of three separate crucibles and filaments allows for the deposition of up to three different materials either simultaneously or sequentially. The 10 cm Si substrate onto which the metals are deposited is mounted on a rotatable feedthrough behind a stepper motor-controlled linear shutter, which provides a method for depositing with a thickness gradient. A Giedd and Perkins evaporation rate monitor allows controlled deposition. The chamber is currently capable of producing films and is being retrofitted to use an Arduino to control the deposition process more easily.

Thesis Supervisor: Dr. Brandon Hoffman
Title: Professor of Physics

TABLE OF CONTENTS

Chapter 1: History and Development 5
 1.1. Thin Film Production and Research..... 5
 1.2. Deposition..... 5
 1.3. Deposition Rate Monitors 9
 1.4. Vacuum 11
 1.5. The PVD chamber at Houghton University 15

Chapter 2: Theory..... 17
 2.1. Thermionic Emission..... 17
 2.2. Deposition Rate..... 22
 2.3. Deposition Rate Monitor 27

Chapter 3: Apparatus 29
 3.1. Chamber Exterior and Vacuum System 29
 3.2. High Voltage Supply..... 30
 3.3. Chamber Interior 31
 3.3.1. Shutters..... 31
 3.3.2. Evaporator 32
 3.3.3. Substrate Holder 35
 3.3.4. Deposition Rate Monitor 36

Chapter 4: Experiment and Results..... 37

Chapter 5: State of the Chamber and Future Work..... 39

TABLE OF FIGURES

Figure 1. Diagram of Grove’s sputtering apparatus	7
Figure 2. Diagram of multiple target deposition	8
Figure 3. Diagram of H. M. O’Bryan’s apparatus	9
Figure 4. Diagram of evaporation rate monitor developed by Giedd and Perkins.....	11
Figure 5. Diagram of Robert Boyle’s pump design.....	12
Figure 6. Diagram of Sprengel Pump.....	13
Figure 7. Diagram of Barnes’s rotary pump	14
Figure 8. W. Becker’s Turbomolecular pump	14
Figure 9. Diagram of allowed electron states in a cube in quantum number space	18
Figure 10. Diagram of particle density through a plane	22
Figure 11. Diagram of deposition geometry.....	26
Figure 12. Picture of the chamber exterior.....	29
Figure 13. Schematic of high voltage circuit.....	30
Figure 14. Oscilloscope trace of output AC voltage	31
Figure 15. Diagram of the chamber interior.....	32
Figure 16. Image of evaporator system.....	33
Figure 17. Schematic of ceramic evaporator base	33
Figure 18. Schematic of steel rod.....	34
Figure 19. Schematic of tantalum crucible holder	34
Figure 20. Schematic of graphite crucible	35
Figure 21. Images of substrate holder	36
Figure 22. Image of deposition rate monitor	36
Figure 23. Image of Ag film on Si substrate	37

Chapter 1

HISTORY AND DEVELOPMENT

1.1. Thin Film Production and Research

Thin films are typically referred to as a substance or layer of material with a thickness ranging from a fraction of a nanometer to even 5 μm thick, though films can be considered thick or thin based on if their properties are more bulk-like or surface-like. Thin films are useful in many different applications, such as semiconductor devices, photoconductors, multilayer capacitors, computer chips, and more.

One of the main reasons why thin films have such a large number of applications is because their properties can easily be controlled and changed to meet desired specifications. Thin films are a polycrystalline material composed of grains, which are a three-dimensional lattice of the deposited particles. Through experimenting with the creation of films using different deposition methods and rates, it has been found [1, 2, 3, 4] that both the deposition rate and film thickness relate to the grain size of the produced films. Furthermore, the grain size contributes to the thermoelectrical properties of the films, where a larger grain size leads to an increase in crystallinity and therefore thermal and electrical conductivity. Of course, this can still vary from metal to metal, and if the thickness of the film becomes too great, the film can begin to lose its film-like properties, resulting in a decrease in its thermoelectrical capabilities. Because the thermoelectrical properties can depend heavily on deposition parameters, many methods of deposition have been developed over the years.

1.2. Deposition

Thin film production has been accomplished in many ways over the last couple centuries, such as spin coating, chemical vapor deposition (CVD), atomic layer deposition (ALD), and physical vapor deposition (PVD). Each of these methods is capable of producing metal films.

Spin coating, first proposed [5] in 1958, involves applying a solution onto a substrate which is then rotated at a high speed. This rotation is continued as the film spreads over the substrate and subsequently spins off until the intended thickness is reached. While this

method is fairly simple and cost effective, it requires the deposited substance to be a fluid and wastes most of the fluid placed on the substrate.

CVD involves the use of chemical reactions to vaporize a desired material which subsequently condenses on a substrate. The first implementation of this process was performed in 1880 by William E. Sawyer and Albon Man [6] who evaporated carbon by immersing it in a hydrocarbon and heating it to extreme temperatures. This resulted in the deposition of the carbon onto filaments for use in electric lamps.

ALD involves several highly reactive precursor chemicals, each of which contains different elements of the desired deposit material. Each of these precursor materials is introduced separately, allowing the film growth to be self-limiting. The first experiments [7] involving ALD were successful in achieving this goal, resulting in mostly uniform films. The primary benefit of ALD is the conformality of the films. Choosing to increase the duration of the reaction allows said reaction to take place on the entire surface of the film, resulting in a uniform film layer. However, ALD is a very slow process and requires an ultra-clean surface onto which the film is deposited.

PVD involves three main steps: vaporizing a target material, transportation from the target to the substrate, and condensation of the vapors leading to film nucleation. Sputtering is a form of PVD that involves bombarding a target with ions. Atoms of the target material are knocked off and travel to the substrate to condense into a thin film. The earliest record [8] of sputter deposition was made in 1852 by W. R. Grove. Grove's apparatus (Figure 1) used a transformer built by M. Ruhmkorff powered by a nitric acid battery to discharge current between a steel needle and a copper plate with an electroplated silver surface. The discharge between the needle and plate ionized the gas between them, resulting in a thin oxide film.

Evaporation, another method of PVD, was probably first accomplished [9] in 1857 by Michael Faraday. In his experiments, Faraday quickly provided a large current to a thin gold wire using Leyden batteries. This method, a form of what is now known as resistive heating, quickly vaporized the gold, depositing it on surfaces made of various materials. Recently, it has become common to use resistive heating boats [10, 11, 12, 13], evaporating the target

material. Because many metals are highly conductive, resistively generating enough heat to melt and subsequently evaporate the metal is more difficult than simply heating a different substance in contact with the target material. However, depending on the latent heat of vaporization of the target material, the temperature of the heating element can be considerably higher than that of the target. This can lead to issues with evaporation, such as the target forming an alloy with the heating element.

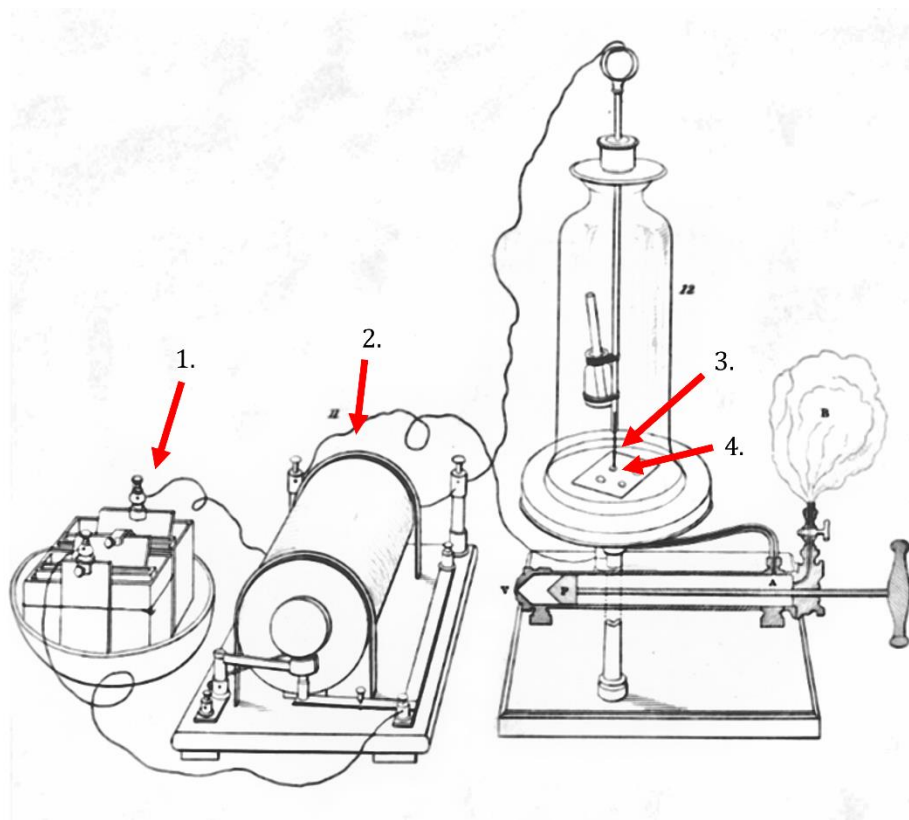


Figure 1. Diagram of Grove's sputtering apparatus. The battery (1.) provides power for the apparatus and the transformer (2.) increases the voltage. The steel needle (3.) ionizes the air molecules between it and the copper plate with silver surface (4.). Figure taken from Ref. [8].

Electron beam heating [14, 15] is another method of heating used for evaporation. A thermionic gun utilizes a heated wire or disk as the cathode to emit electrons. With thermionic guns, it is possible to introduce electric and magnetic fields to control the path of the electrons. However, thermionic guns are hindered in that they require lower pressures, about 10^{-3} Torr to operate at full functionality, as higher pressures can cause the electron beam to scatter or reduce the life of the cathode. Plasma guns rely on ionizing a desired gas,

and these ions strike the cathode, releasing the necessary electrons. Both types of guns can be used to equal effect for evaporation. The primary downside for these methods is controlling the beam that hits the material. The beam must be controlled in a way that the beam is able to heat the material without interfering with the evaporated metal.

Deposition due to evaporation has developed at an extraordinary rate and has many benefits over methods like CVD. For example, it is possible to use multiple evaporation targets to create either a layered or alloy coating (see Figure 2) as performed 1993 by J. R. Nicholls et al. [16]. In the experiment, they used multiple targets to evaporate Ni, Cr, and Al simultaneously, allowing the metals to mix during the vapor phase of deposition. This allows for the creation of a vast array of material combinations. These combinations may then be studied to determine the optimal characteristics for a given application. Evaporation can also be used for higher deposition rates, as the rate is not directly related to the rate of chemical reactions. Furthermore, the ability to control more deposition parameters over CVD allows more control in the formation, nucleation, and growth of the film.

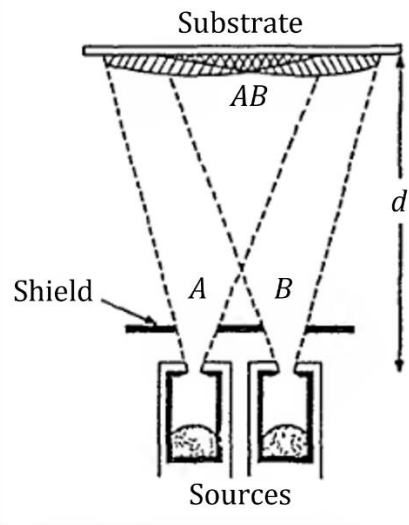


Figure 2. Diagram of multiple target deposition. Target materials *A* and *B* are evaporated and mix in the vapor phase. At small distances *d* from the substrate, only the center area will be alloyed or layered (*AB*). This can be remedied by putting the targets closer together, angling both directly towards the substrate for complete overlap, or increasing the distance *d*. Figure taken from Ref. [17].

While many deposition methods involved directly heating the substance to be evaporated, H. M. O'Bryan came up with the idea to hold the target material in a graphite crucible [18] (see Figure 3). This crucible is then heated through thermionic emission, which involves bombarding the crucible with electrons from a tungsten filament coil surrounding the crucible. This eliminated the issue of the target metal alloying with the heating element by separating the two, as well as issues arising from the heating element having significantly greater temperatures than the target. While it is possible to resistively heat a graphite crucible [19], this method requires a very high current. In testing the apparatus, O'Bryan evaporated several materials such as molybdenum, boron, and platinum, as well as carbon and boron and silicon carbide. None of the materials tested reacted much with the crucible, at most forming a layer of carbide between the crucible and target material, preventing further reaction. However, when evaporating carbon in the crucible, the crucible partially melted at around 3500°C.

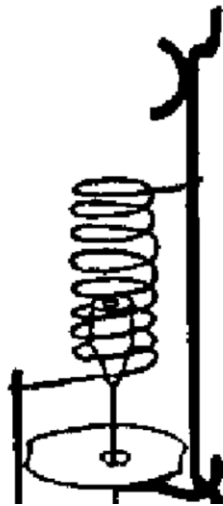


Figure 3. Diagram of H. M. O'Bryan's apparatus. The surrounding coil bombards the crucible with electrons, heating and evaporating the target material. Figure taken from Ref. [18].

1.3. Deposition Rate Monitors

Knowing the rate of deposition is very important if precisely controlled deposition is desired. The quartz-crystal microbalance (QCM) [20], invented in 1959 by Günter Sauerbrey, has been a very popular method for evaluating deposition rate for decades, simply because of how accurately it is able to measure the rate of deposition. The quartz crystals used in QCMs

experience the piezoelectric effect. When a material is subject to this effect, a mechanical stress results in the creation of an external electric field. This effect may also be applied in reverse, whereby applying an electric field will stretch or compress the material. The application of an alternating current will induce oscillations in the crystal. Furthermore, the frequency of these oscillations is inversely proportional to the thickness of the crystal, so when a material is deposited on the surface of the crystal, causing the thickness to increase, the oscillation frequency will decrease. It is then possible to correlate this change in frequency with the thickness of the deposited material, and the change in thickness can be determined with an accuracy of about a nanogram per square centimeter. However, the main issue with QCMs is that over time, as more material is deposited on the surface of the quartz crystal, the resonant frequencies slowly change. Because of this, it becomes necessary to replace the crystal regularly.

In 1960, G. R. Giedd and M. H. Perkins [21], developed an evaporation rate monitor (see Figure 4) that measured the ionization rate occurring, which was experimentally determined to be directly related to the deposition rate. Because of this relationship, the device allows the deposition of a given material while controlling the overall thickness of the deposit. Giedd and Perkins found that maximum ionization probability occurred when the anode had a potential of 155 V, the collector had a potential of -20 V, and the filament carried a current of 40 mA. The device was calibrated by heating and stabilizing the target material until a constant ion current was indicated. Then, the material was permitted to deposited for a controlled amount of time, and the ion current was plotted against the deposition rate (Figure 4).

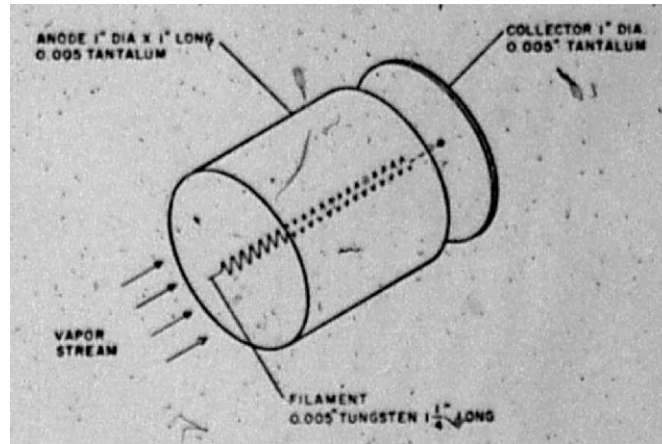


Figure 4. Diagram of evaporation rate monitor developed by Giedd and Perkins. The device consists of a powered filament surrounded by a cylindrical anode and a collector plate. The filament supplies the ionizing electrons, the anode accelerates the ions, and the collector plate collects the ions and produces current based on the number of ions collected. Figure taken from Ref [21].

1.4. Vacuum

The vacuum is one of the most important aspects of many deposition methods and therefore the creation of thin metal films. In the 1640s, Otto von Guericke was one of the first scientists to make headway in the various attempts to achieve a low enough pressure to call a “vacuum.” While the concept of vacuums had been around for a while, not many attempts had fully proved that it was possible to remove much air from a given space. In one of his first experiments, Guericke affixed a large copper sphere to a piston pump and had some men attempt to pump all the air from the sphere [22]. To accomplish this, a piston would be pulled down through a tube, creating a low-pressure region. The valve between the tube and chamber would be opened, allowing air from the chamber to rush into the tube, and closed again. A stopper would then be removed and the piston pushed up to its original position, expelling any air in the tube. The stopper would be placed back in, preventing any air from entering the tube from the outside while beginning the process again. As Guericke and the men pumped away and began feeling confident that all the air had been extracted, they were suddenly terrified as, with an extremely loud sound, the metal sphere imploded. Guericke reasoned that the external air pressure was far too great, and the imperfect globe collapsed upon itself. Shortly after, the experiment was repeated with a more accurately constructed sphere, and while the sphere did not implode, Guericke noted that the air became more

difficult to pump out over time. These experiments ultimately proved to the world that creating at least an approximate vacuum was possible.

In 1658, Robert Boyle attempted to design a more efficient vacuum pump [23] (see Figure 5) that could more easily evacuate a vessel. The fundamental process of pumping the air out was very similar to von Guericke's pump, but what made this design so effective was the use of a rack and pinion system for pumping, making pumping to lower pressures significantly easier. Boyle's pump was able to achieve 6 Torr.



Figure 5. Diagram of Robert Boyle's pump design. The image on the left shows the apparatus and the image. This image on the right shows the process by which air is evacuated. Figure taken from Ref. [24].

Over the next couple centuries, while improvements were made to the piston pump design, most of these improvements simply made the pumps easier to use. Typically, this involved shortening the time taken to lower the pressure. In the mid-1800s, Dr. Hermann Sprengel

[25] designed a pump that used droplets of mercury to evacuate air (see Figure 6). Sprengel used a long, thin tube connected to the chamber to be evacuated, and the air would expand into the tube. Then, by using a funnel, Sprengel poured mercury down the tube, forcing down any air that had expanded into it. While the process was slow, the pump was able to achieve a pressure of approximately 8×10^{-4} Torr.

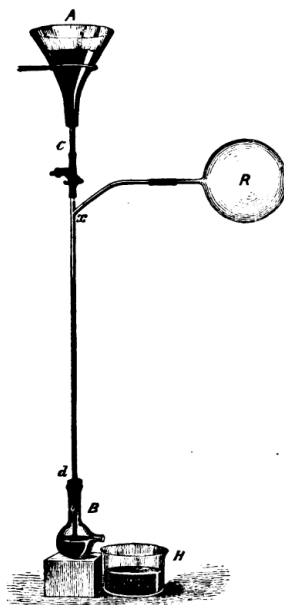


Figure 6. Diagram of Sprengel Pump. Mercury was poured into funnel *A* and, providing stop-cock *c* was open, ran down the tube from *x* to *d*. This would trap small amounts of air that had expanded from *R* and drag the air down to the spout of bulb *B* to be released. Figure taken from Ref. [25].

In 1874, Charles C. Barnes filed a patent [26] for a rotary pump, which uses a rotor inside a cavity. The rotor has several grooves with a vane in each. These vanes correspond in length to the diameter of the cavity for any line through the center of the rotor and have a small amount of sliding movement. These factors allow both ends of the vanes to maintain contact with the cavity wall at all time, and the rotating of the vanes provides continuous suction (see Figure 7). While the pump was able to achieve a pressure similar to Sprengel's Pump, the system was substantially easier to operate.

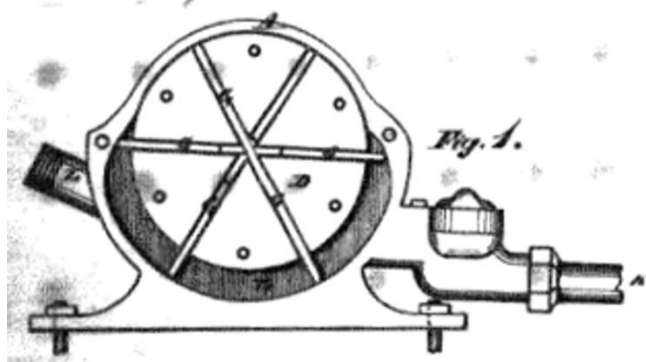


Figure 7. Diagram of Barnes's rotary pump. By rotating the vanes rapidly, it is possible to create continuous suction through the device. Figure taken from Ref. [26].

In 1957, Willi Becker [27] chose to design the turbomolecular pump based on Wolfgang Gaede's molecular pump design from 1913. Becker's pump (see Figure 8) contains both stationary stator blades and blades attached to a central rotor, and by spinning, the rotor blades give momentum to the gas being pumped, forcing them into the next set of blades. This process essentially funnels the molecules in the desired direction, typically towards a pump. However, the turbomolecular pump requires a backing pump to reach its optimal starting pressure of around 10^{-3} Torr, and after this, it is possible to reach pressures of about 10^{-8} Torr.

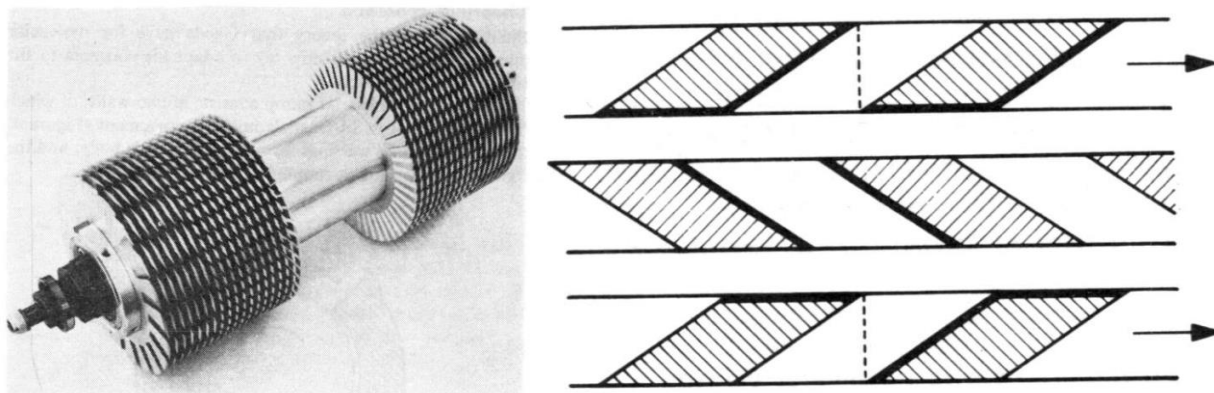


Figure 8. W. Becker's Turbomolecular pump. On the right is a diagram of the rotor system. The rotary blades push the air down through the stator blades into the next set of rotary blades. Figure taken from Ref. [27].

The sputter ion pump (SIP), patented [28] in 1961, was designed to maintain a vacuum of about 10^{-8} Torr. Similar to the turbomolecular pump, SIPs typically require a backing pump to lower the pressure before use to around 10^{-4} Torr. The operation of most ion pumps is reliant on a Penning trap, which is a device used to store charged particles using a magnetic and electric field. By using an electrical discharge, electrons are confined within the Penning trap and ionize gas molecules that enter. These newly formed ions are accelerated towards and strike a cathode, which sputters cathode material onto the inside walls of the pump. This layer of cathode material then absorbs the gas through the formation of bonds, reducing the gas pressure inside the chamber and maintaining an ultra-high vacuum.

The titanium sublimation pump [29], designed in 1966 uses a similar concept to the SIP. By inducing a high current through a titanium filament, the filament is able to reach titanium's sublimation temperature. By sublimating the filament, a thin layer of clean titanium is deposited on the walls of the chamber, reacting with the gas in a similar way to the SIP. The pump is able to operate starting at pressures of 10^{-3} Torr down to below pressures of 10^{-11} Torr. However, this method has some slight drawbacks. Firstly, the thin film of titanium on the walls will become less clean over time as the gas and titanium form bonds. This simply means that the filament must be sublimated once more to form a clean layer. Furthermore, the filament will slowly lose material until it is no longer usable, in which case it must be replaced.

1.5. The PVD chamber at Houghton University

The PVD chamber at Houghton University houses a recently constructed evaporation system that deposits up to three metals simultaneously or sequentially. This is accomplished by using three separate graphite crucibles, each above a corresponding tungsten filament. A high negative voltage can be imparted through each filament, leading to the thermionic emission which heats the crucibles. Following evaporation of the chosen metal, a thin film is formed on a substrate mounted on the chamber ceiling. The method of thermionic emission heating was chosen for its simplicity and cost-effectiveness compared to other methods such as CVD or ALD, though it is still an effective method for deposition. Before deposition may

occur, the chamber is pumped down using a rotary and turbomolecular. Once again, these pumps were chosen due to the combination of their effectiveness and ease of use.

At Houghton University, the deposition chamber is but one project related to thin films. Other students are working on an x-ray diffractometer [30], interferometer [31], and scanning tunneling microscope [32]. Each of these three devices are being worked on with the intention of studying the thin films the deposition chamber creates, specifically to determine how different deposition parameters affect the film's grains and its attributes. By studying the film's grains and their relation to deposition parameters it will be possible to determine correspondence between the two. Additionally, it will be beneficial to study how annealing parameters change the film and its properties.

Chapter 2

THEORY

2.1. Thermionic Emission

The deposition chamber's crucible is heated through the process of thermionic emission from a tungsten filament. Heating the crucible results in the evaporation of the target material therein, which is necessary for the deposition process. Thermionic emission is the process by which an electrode is heated to a high temperature, providing the electrons sufficient energy to overcome the material's work function.

The Fermi-Dirac distribution function represents the probability that a given energy state having energy E is occupied by an electron:

$$f(E) = \frac{1}{e^{\frac{(E-E_F)}{k_B T}} + 1}. \quad (1)$$

In this equation, E_F is the Fermi energy, k_B is Boltzmann's constant, and T is the absolute temperature in K. Now, the energy of an electron in a cube of sides L and volume L^3 is

$$E = \left(\frac{\hbar^2 \pi^2}{2m_e L^2} \right) (n_x^2 + n_y^2 + n_z^2), \quad (2)$$

where m_e is the mass of an electron. If an electron is confined within a three-dimensional cube and restricted to boundary conditions in all three dimensions, then the allowed states of such an electron may be represented in a quantum number space. The axes in the quantum number space would be represented by n_x , n_y , and n_z . The permitted electron states in a quantum space such as this may be represented as dots at integral values of the quantum numbers (see Figure 9).

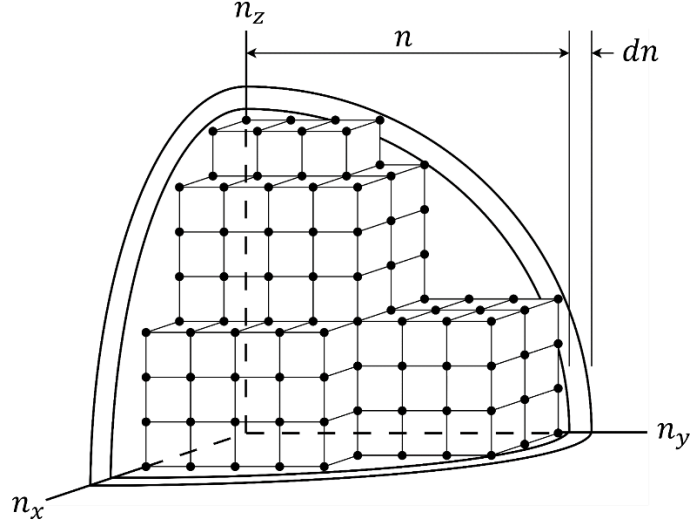


Figure 9. Diagram of allowed electron states in a cube in quantum number space. The dots represent allowed states at integer values of n_x , n_y , and n_z . The number of allowed states with energies between E and $E + dE$ corresponds to the number of points in the shell of radius n and thickness dn .

It is possible to define

$$E_0 \equiv \frac{\hbar^2 \pi^2}{2m_e L^2} \text{ and } n \equiv (n_x^2 + n_y^2 + n_z^2)^{\frac{1}{2}} \quad (3)$$

and rewrite Equation (2) as

$$\frac{E}{E_0} = n^2, \quad (4)$$

which can be used to represent the sphere of radius n in the quantum space. The number of allowed states with energies between E and $E + dE$ is then equivalent to the number of points in the shell of radius n and thickness dn . The volume of said shell represents the total number of states $G(E) dE$:

$$G(E) dE = \frac{1}{8} (4\pi n^2) dn = \frac{1}{2} \pi n^2 dn. \quad (5)$$

The volume must be $\frac{1}{8}$ of the total for the sphere, because the states are restricted to the octant of quantum space where all three quantum numbers are positive. The equivalent for n in terms of E from Equation (3) allows the differential to be evaluated:

$$G(E) dE = \frac{1}{4} \pi E_0^{-\frac{3}{2}} E^{\frac{1}{2}} dE. \quad (6)$$

Using E_0 from Equation (3) and dividing by $V = L^3$, the volume of the box in normal space, it is possible to find the number of allowed energy states per unit volume:

$$g(E) dE = \frac{G(E)}{V} dE = \frac{\sqrt{2} m_e^{\frac{3}{2}}}{2 \hbar^3 \pi^2} E^{\frac{1}{2}} dE. \quad (7)$$

This must then be doubled to account for the possible spin states, resulting in

$$g(E) dE = \frac{\sqrt{2} m_e^{\frac{3}{2}}}{\hbar^3 \pi^2} E^{\frac{1}{2}} dE. \quad (8)$$

The density of electrons per unit volume that have energy between E and $E + dE$ is defined as the number of allowed states multiplied by the probability that a state is occupied, which can be written as

$$N(E) dE = g(E) f(E) dE = \left(\frac{\sqrt{2} m_e^{\frac{3}{2}}}{\hbar^3 \pi^2} E^{\frac{1}{2}} \right) \left(\frac{1}{e^{\frac{(E-E_F)}{k_B T}} + 1} \right) dE. \quad (9)$$

By using $\hbar \equiv \frac{h}{2\pi}$, and the nonrelativistic energy of an electron, $E = \frac{1}{2} m_e v^2$, the equation simplifies to

$$N(E) dE = \frac{2m_e^3}{h^3} e^{\left(\frac{\frac{1}{2} m_e v^2 - E_F}{k_B T} \right)} 4\pi v^2 dv. \quad (10)$$

The thermal emission current density is defined as

$$J_z = \int_{E \geq E_{min}} e v_z(E) N(E) dE, \quad (11)$$

where e is the charge of an electron and $v_z(E)$ is the electron velocity distribution perpendicular to the surface of the emitting metal. Furthermore, the integral must be evaluated for energies sufficient to escape the potential barrier, $E \geq E_{min} = W + E_F$. Applying the fact that $v^2 = v_x^2 + v_y^2 + v_z^2$ and $4\pi v^2 \rightarrow dv_x dv_y dv_z$, the current density can be expressed as

$$J_z = \frac{2em_e^3}{h^3} e^{\frac{E_F}{k_B T}} \int_{-\infty}^{\infty} e^{-\frac{m_e v_x^2}{2k_B T}} dv_x \int_{-\infty}^{\infty} e^{-\frac{m_e v_y^2}{2k_B T}} dv_y \int_{v_{z,min}}^{\infty} e^{-\frac{m_e v_z^2}{2k_B T}} dv_z. \quad (12)$$

Evaluating this integral results in

$$J_z = \frac{2em_e^3}{h^3} e^{\frac{E_F}{k_B T}} \frac{\pi 2k_B T}{m_e} \frac{e^{-\frac{m_e v_{z,min}^2}{2k_B T}}}{\frac{m_e}{k_B T}} = \frac{4em_e \pi k_B^2}{h^3} T^2 e^{\frac{W}{k_B T}}, \quad (13)$$

which is also known as the Richardson-Dushman equation [33], first derived by Owen Willans Richardson. It is more commonly simplified as

$$J = A_0 T^2 e^{\frac{-W}{k_B T}}, \quad (14)$$

where

$$A_0 \equiv \frac{4\pi e m_e k_B^2}{h^3} = 1.2 \times 10^6 \frac{\text{A}}{\text{m}^2 \text{K}^2}. \quad (15)$$

Using the current density, it is possible to determine the thermionic current, which is simply the product of the current density and the surface area of the coiled tungsten filament,

$$I = 2\pi r l A_0 T^2 e^{\frac{-W}{k_B T}}, \quad (16)$$

where r and l are the radius and length of the coil, respectively. It is also important to know the power emitted from the filament, which may be expressed as

$$P_f = 2\pi r l A_0 V T^2 e^{\frac{-W}{k_B T}}, \quad (17)$$

where V is the potential difference between the filament and the crucible. As can be seen in the equation, the thermionic power is exponentially dependent on the temperature of the filament.

Finally, it is important to note that the temperature of the metal being evaporated, T_e , is dependent on the thermionic power. This can be approximated by assuming that the system is at an equilibrium, meaning that $\frac{dP}{dt} = 0$. The three main forms of power involved are the thermionic power absorbed (Equation (17)) as well as the release of radiated power,

$$P_r = \varepsilon \sigma A_e T_e^4, \quad (18)$$

where ε is the emissivity, σ is the Stefan-Boltzmann constant, A_e is the area of the surface area of the evaporated material, and T_e is the temperature of the evaporated material, and conductive power,

$$P_c = kA \frac{dT}{dx}, \quad (19)$$

where k is the thermal conductivity, A is the contacting surface area of contact, and $\frac{dT}{dx}$ is the rate at which temperature changes with position. The conductive power lost would theoretically need to be calculated out from the evaporated material to the chamber itself. By evaluating

$$0 = P_f - P_r - P_c, \quad (20)$$

it would be possible to determine the temperature of the material being evaporated. Because the temperature is dependent on the thermionic power, the evaporation rate, and therefore deposition rate, must also be dependent on the thermionic power.

2.2. Deposition Rate

The number of particles with velocity v passing through a plane in time Δt can be described with a cylinder with length equal to the distance travelled by the stream of particles with area A (see Figure 10):

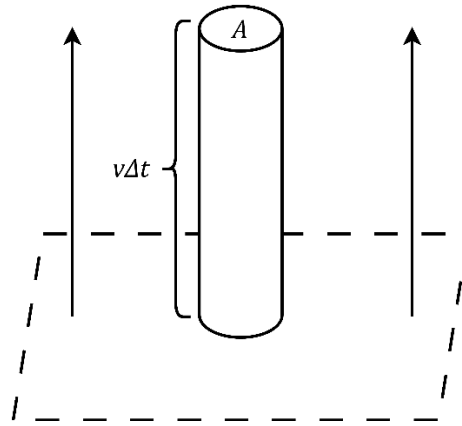


Figure 10. Diagram of particle density through a plane. A number of particles, N , passing through area A of a plane in time Δt with velocity v .

$$N = \rho Av\Delta t, \quad (21)$$

where ρ is the number of particles divided by the volume. The Maxwell-Boltzmann distribution for particles moving in one dimension is

$$f(v)dv = \sqrt{\frac{m}{2\pi k_B T}} e^{-\left(\frac{mv^2}{2k_B T}\right)} dv, \quad (22)$$

where m is the mass of the moving particles. This can be used to find the number of particles travelling in such a cylindrical volume:

$$N = \rho A \Delta t \sqrt{\frac{m}{2\pi k_B T}} \int_0^\infty v e^{-\left(\frac{mv^2}{2k_B T}\right)} dv. \quad (23)$$

integrating the function yields a more adequate estimation for the number of particles in the cylinder:

$$N = \rho A \Delta t \sqrt{\frac{m}{2\pi k_B T}} \left(\frac{k_B T}{m}\right) = \rho A \Delta t \sqrt{\frac{k_B T}{2\pi m}}. \quad (24)$$

From the Ideal Gas Law,

$$\rho = \frac{P}{k_B T}, \quad (25)$$

where P is the pressure of the gas. Using this yields

$$N = \frac{P}{k_B T} A \Delta t \sqrt{\frac{1}{2\pi m}} = P A \Delta t \sqrt{\frac{1}{2\pi m k_B T}}. \quad (26)$$

Equation (26) may then be rewritten as the rate of particles per unit area that travel across a plane,

$$\frac{dN}{A dt} = P \sqrt{\frac{1}{2\pi m k_B T}}. \quad (27)$$

When evaluating the evaporation of a substance, it is important to include a variable, α_e , to represent the probability of a phase change occurring through particles evaporating,

$$\frac{dN_e}{A dt} = \alpha_e P_h \sqrt{\frac{1}{2\pi m k_B T}}, \quad (28)$$

where N_e is the number of evaporating molecules and P_h is the hydrostatic pressure acting on the surface. This must also be done for particles condensing using α_c :

$$\frac{dN_c}{A dt} = \alpha_c P^* \sqrt{\frac{1}{2\pi m k_B T}}, \quad (29)$$

where N_c is the number of condensing molecules and P^* is the equilibrium vapor pressure of the target at its surface. Assuming that the probabilities of evaporation and condensation are equivalent, $\alpha_e = \alpha_c \equiv \alpha_v$, the equation may finally be rewritten in the form of the well-known Hertz-Knudsen [17] equation,

$$\frac{dN_{net}}{A_t dt} = \frac{\alpha_v}{\sqrt{2\pi m k_B T}} (P^* - P), \quad (30)$$

where dN_{net} is the net number of molecules evaporating from the target's surface area, A_e in time dt , and α_v is the evaporation coefficient, which is the ratio of the actual evaporation rate in a vacuum to the theoretically possible value. In this case, α_v depends on how clean the surface of the target is. If evaporating a target with a fresh, clean surface, then $P_h \ll P^*$ and $\alpha_v = 1$. This would mean that

$$\frac{dN_{net}}{A_e dt} = \frac{P^*}{\sqrt{2\pi m k_B T}}. \quad (31)$$

The vapor pressure in atm for a metallic element can be described with [34]

$$\log P^* = A + \frac{B}{T} + C \log T + \frac{D}{T^3} \quad (32)$$

where P^* is in atm and A, B, C , and D are real constants that depend on the evaporated material. Equation (32) can then be solved for P^* and inserted into Equation (31), resulting in

$$\frac{dN_{net}}{A_e dt} = \frac{1}{\sqrt{2\pi m k_B T}} \left(e^{A + \frac{B}{T} + C \log T + \frac{D}{T^3}} \right). \quad (33)$$

It is possible to determine the mass evaporation rate per unit area, Γ , by multiplying Equation (33) by the mass of an individual molecule of the target, resulting in

$$\Gamma = m \frac{dN_{net}}{A_e dt} = \sqrt{\frac{m}{2\pi k_B T}} \left(e^{A + \frac{B}{T} + C \log T + \frac{D}{T^3}} \right). \quad (34)$$

The total amount of evaporated material, \mathcal{M}_e , may be found utilizing Γ in the following double integral:

$$\mathcal{M}_e = \int_t \int_{A_e} \Gamma dA_e dt. \quad (35)$$

While the above equations simply cover how many molecules leave the surface of a target material, it is also important to consider into which direction the particle is emitted. Because the distance to the receiving surface is much larger than the target material, it can be assumed that the target is an infinitesimally small point of surface area dA_e . In this case, provided the vaporized molecules have a Maxwellian speed distribution at departure, the mass evaporation rate will be uniform in all directions, as shown in Figure 11. Therefore, the mass of evaporated material within a narrow beam of solid angle of increments $d\omega$ is

$$d^3 \mathcal{M}_e = \Gamma dA_e dt \frac{d\omega}{4\pi}, \quad (36)$$

and inserting Equation (35) results in

$$d\mathcal{M}_e = \mathcal{M}_e \frac{d\omega}{4\pi}. \quad (37)$$

The receiving surface area element, dA_r , that corresponds to solid angle $d\omega$ is

$$dA_r = \frac{r^2 d\omega}{\cos \theta}, \quad (38)$$

where θ is the angle between the incident angle of deposition and the normal to the receiving surface as seen in Figure 11. This provides the deposit mass received per unit area,

$$d\mathcal{M}_r = \frac{\mathcal{M}_e \cos \theta}{4\pi r^2} dA_r. \quad (39)$$

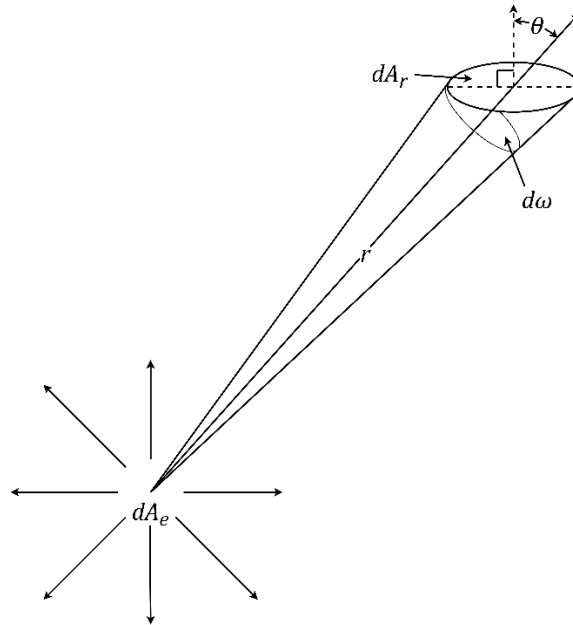


Figure 11. Diagram of deposition geometry. Deposition from surface area dA_e onto surface area dA_r . $d\omega$ is the solid angle that corresponds with the receiving surface.

To find the rate of deposition in terms of thickness per unit time, it is necessary to solve Equation (35), using the results to subsequently solve Equation (39). This can then be divided by the result by the density of the deposited material, resulting in the volume of material received, V_r ,

$$V_r = \frac{\sqrt{\frac{m}{2\pi k_B T}} \left(e^{A + \frac{B}{T} + C \log T + \frac{D}{T^3}} \right) A_e A_r \cos \theta}{4\pi r^2 \rho_e} \cdot t, \quad (40)$$

which can then be divided by the area of the receiving surface for height, or in this case thickness, x_r , as a function of time,

$$x_r = \frac{\sqrt{\frac{m}{2\pi k_B T}} \left(e^{A + \frac{B}{T} + C \log T + \frac{D}{T^3}} \right) A_e \cos \theta}{4\pi r^2 \rho_e} \cdot t. \quad (41)$$

Using this, it is possible to determine the amount of material deposited in a given amount of time. It is important to note that the amount of target material deposited in a given location is exponentially related to the temperature and inversely proportional to the square of the distance from the target to the recipient surface. Furthermore, because the deposition is not solely perpendicular to the receiving surface, the thickness of the deposit will form a gradient. Calculating the rate of deposition and thickness of the film is beneficial, but far more beneficial is the ability to know the immediate rate of deposition during the deposition process.

2.3. *Deposition Rate Monitor*

The deposition rate monitor used in the Houghton deposition chamber is very similar to the apparatus designed by Giedd and Perkins [21]. The monitor measures the ionization rate occurring in the system, which was found to be dependent on the evaporation rate of the target. As discussed in Section 1.3, the monitor consists of a filament to supply ionizing electrons, a cylindrical anode to accelerate the ions, and a circular collector plate. The ionization probability for molecular beams in this and similar geometries has been calculated to be P_i . It is possible to calculate the distribution of vapor from a point source and compare the calculated number of ions to the measured number of atoms deposited on the substrate. By doing this, the ionization probability may be written as

$$P_i = \frac{M I_m}{N_A A_{ped}} \cdot 10^{-8} \quad (42)$$

where M is the molecular mass, I_m is the ion current of the evaporated metal, N_A is Avogadro's number, A is the area of the collector, ρ is the density of the metal, e is the electronic charge, and d is the evaporation rate determined by a measure of the thickness of the film divided by the evaporation time.

Through experimentation, Giedd and Perkins found that the maximum value for ionization probability occurred when the anode potential was 155 V, the collector potential was -20 V, and the electronic current was 40 mA. Furthermore, it was found that with these values, the ion current and deposition rate were linearly related.

Chapter 3

APPARATUS

3.1. Chamber Exterior and Vacuum System

The chamber, as seen in Figure 12, is comprised of an aluminum cylinder 79 cm tall and 28 cm in diameter. On the top of the chamber, a rotary mechanical feedthrough holds the substrate, while an electrical feedthrough connects to an ohmmeter which measures the resistance across the substrate during deposition. On the side of the chamber, a linear feedthrough controls the thickness gradient of the film, and a rotary feedthrough can quickly cover or uncover the substrate. On the bottom of the chamber, a 5-pin electrical feedthrough connects the high voltage supply to the evaporator. There is also a viewing window situated on the side of the chamber to permit observation of the evaporator.

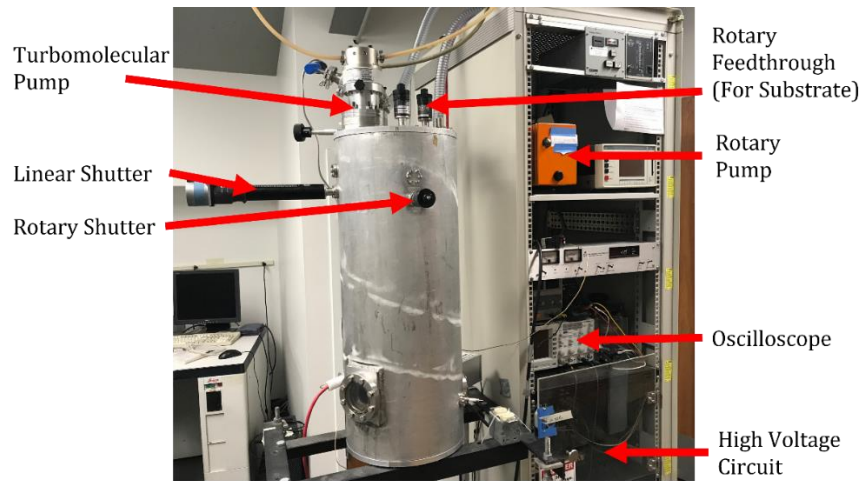


Figure 12. Picture of the chamber exterior. The rotary and turbomolecular pumps bring the chamber to a vacuum of base pressure 10^{-6} Torr, which is determined using an ion gauge. The various feedthroughs aid in controlling the deposition and creation of the films.

Each feedthrough and flange is secured with a Viton O-ring. The chamber is evacuated using an Alcatel 2004a dual stage rotary vane vacuum pump, able to achieve a base pressure of approximately 10^{-3} Torr, backing a Balzers-Pfeiffer TPH-062 Turbomolecular Pump which allows the chamber to reach approximately 10^{-6} Torr after sufficient pumping time.

3.2. High Voltage Supply

The high voltage power supply [35] (Figure 13) designed by Andrew Redman provides both current and high voltage to a tungsten filament. Once at a high enough negative voltage, the filament begins to emit electrons which bombard and heat the crucible. The high voltage circuit is comprised of a Superior Electric Company Powerstat Variable Transformer with two GAL-900U-2 microwave oven transformers (MOTs), whose outputs each connect to a half-wave voltage rectifier and doubler using a diode and a capacitor for each MOT. When the AC voltage is positive, the capacitor will charge, and when the AC voltage is negative, the capacitor will discharge and add to the negative voltage. This output voltage (Figure 14) floats a smaller filament circuit, which provides the filament up to 3 A of current. The two relays drain the circuit if not powered.

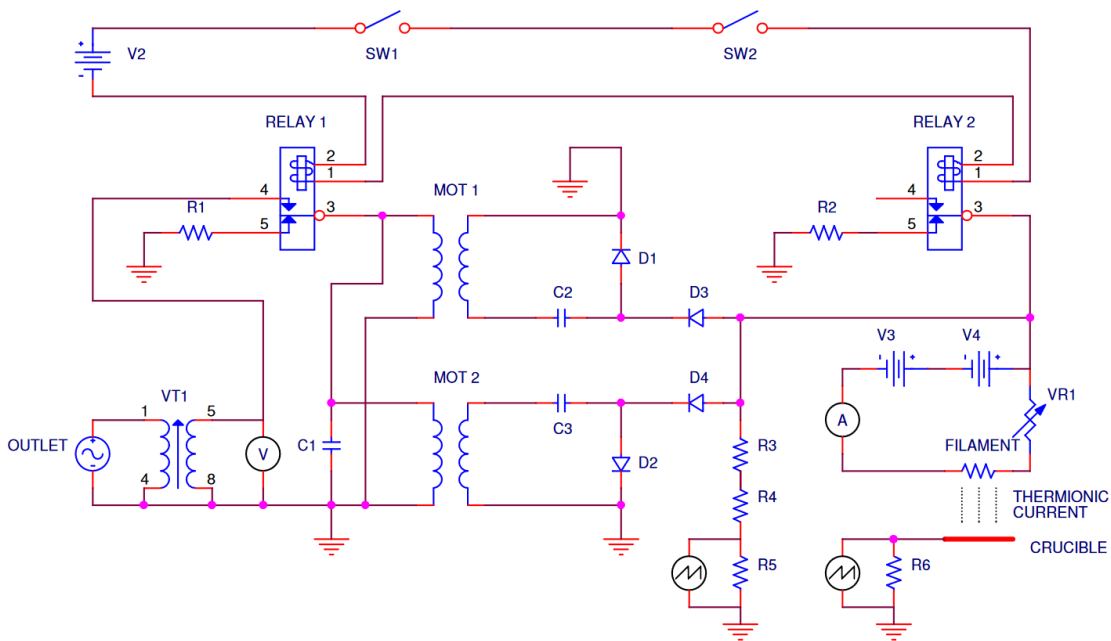


Figure 13. Schematic of high voltage circuit. SW1 and SW2 are interlocking switches on the electrical cabinet doors. Variable transformer VT1 supplies up to 120 V AC at 60 Hz to transformers MOT 1 and 2, each with a 1:20 voltage ratio. MOT 1 and 2 are 180° out of phase and are rectified and doubled through D1, D2, C2, and C3 (both 1 μ F). Diodes D3 and D4 isolate the filament circuit from the lower voltage doubler. The filament voltage is measured using an oscilloscope across R5 (10 k Ω) after being reduced by R3 and R4 (both 47 M Ω). V3 and V4 are both 12 V, and the variable resistor controls the current to the filament which is measured with an ammeter. The thermionic current is found with the oscilloscope measuring the voltage across R6 (1 Ω). R1 and R2 are both 100 Ω , and V2 is 13 V.

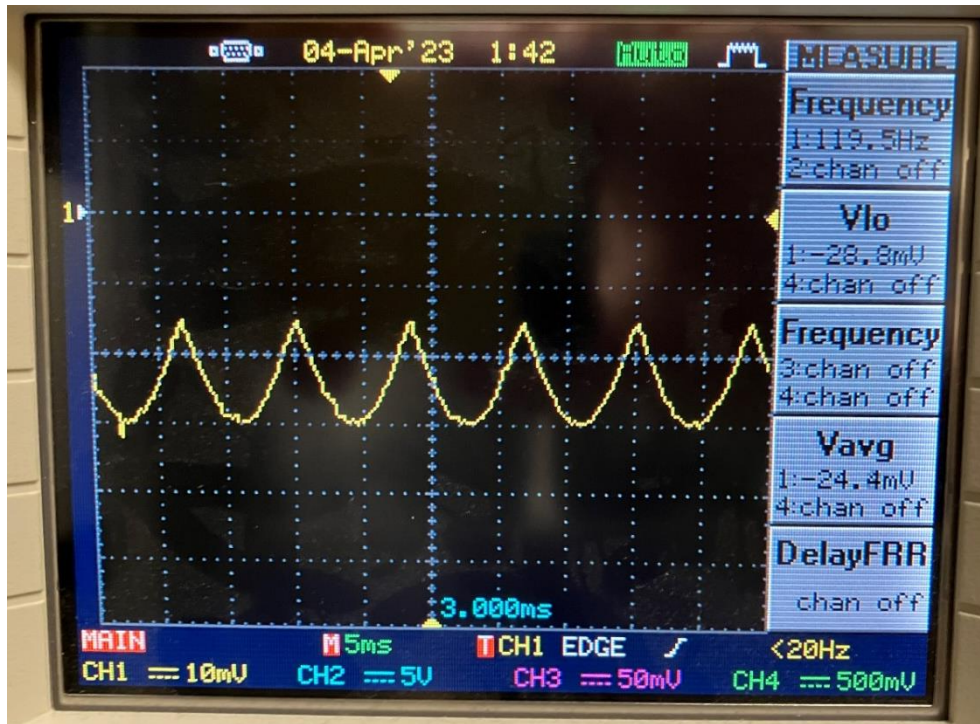


Figure 14. Oscilloscope trace of output AC voltage. The frequency is 120 Hz, because the MOTs are 180° degrees out of phase. Every other valley is a single MOT, and each valley is the combined voltage of an MOT and its corresponding capacitor. The scale is set to 10 mV, because the oscilloscope is reading the voltage after a resistor chain.

3.3. Chamber Interior

3.3.1. Shutters

The chamber contains both a linear and rotary shutter, as depicted in Figure 15. These shutters are implemented to provide better control over the deposition process. The rotary shutter can quickly uncover and cover the substrate, which assists in achieving deposition at a constant rate. The linear shutter controls the thickness gradient of the film using a stepper motor. The evaporator is situated at the bottom of the chamber, mounted on a 5-pin electrical feedthrough.

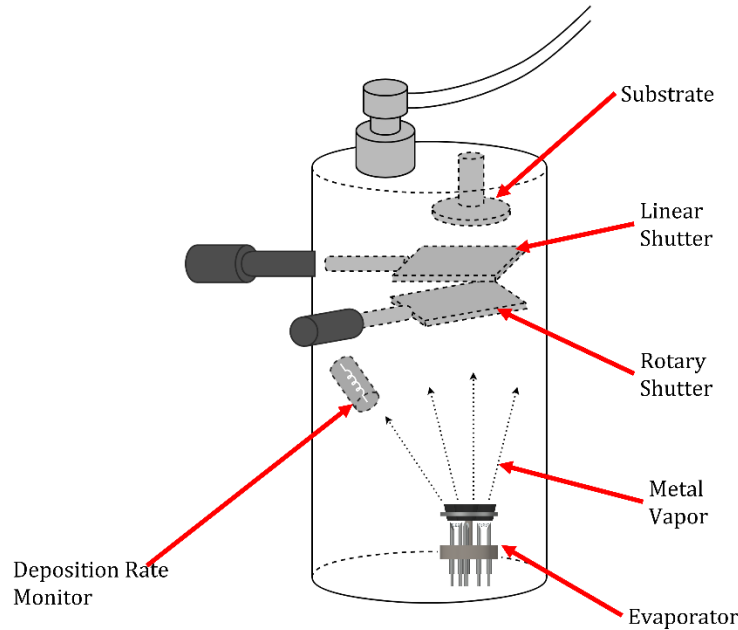


Figure 15. Diagram of the chamber interior. The evaporated metal travels to the silicon substrate, and its thickness and gradient can be controlled using the shutters. The monitor is connected to an oscilloscope to allow control over the rate of deposition.

3.3.2. Evaporator

The evaporator, as seen in Figure 16, consists of several components. The ceramic base (Figure 17) holds the steel rods and screws to which the filaments are spot welded. The filaments are created using 36-gauge tungsten wire wrapped into ten coils with a 2 mm diameter. Because the filaments are provided with a current and high negative potential, the filaments heat up and begin thermionic emission. The emitted electrons are accelerated away from the filament and transfer their kinetic energy to the crucible, heating it and the metal contained within. Each of the three inner rods (Figure 18) acts as the voltage-in pin for their corresponding filament, while the outer fourth rod and the screws are connected to the battery's negative terminal. The tantalum disc (Figure 19) houses the three graphite crucibles (Figure 20) containing the desired metals above the three filaments and connects to the common ground of the transformer circuit.



Figure 16. Image of evaporator system. The system has three crucibles each above a tungsten filament. The goal of the system is to be able to create alloy or layered films by depositing multiple different materials simultaneously or sequentially.

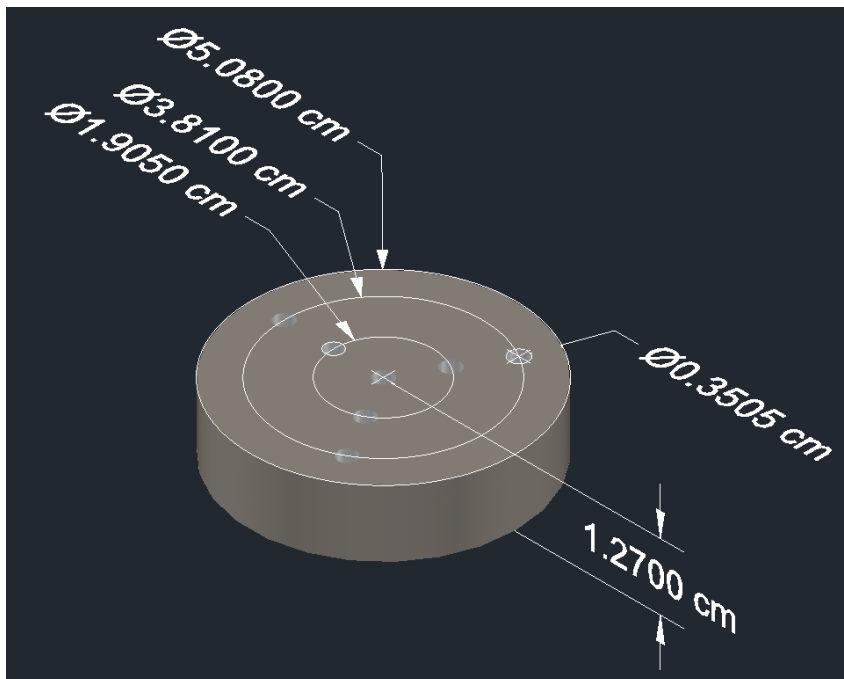


Figure 17. Schematic of ceramic evaporator base. The steel rods and screws are mounted in the radial holes and held with steel nuts.

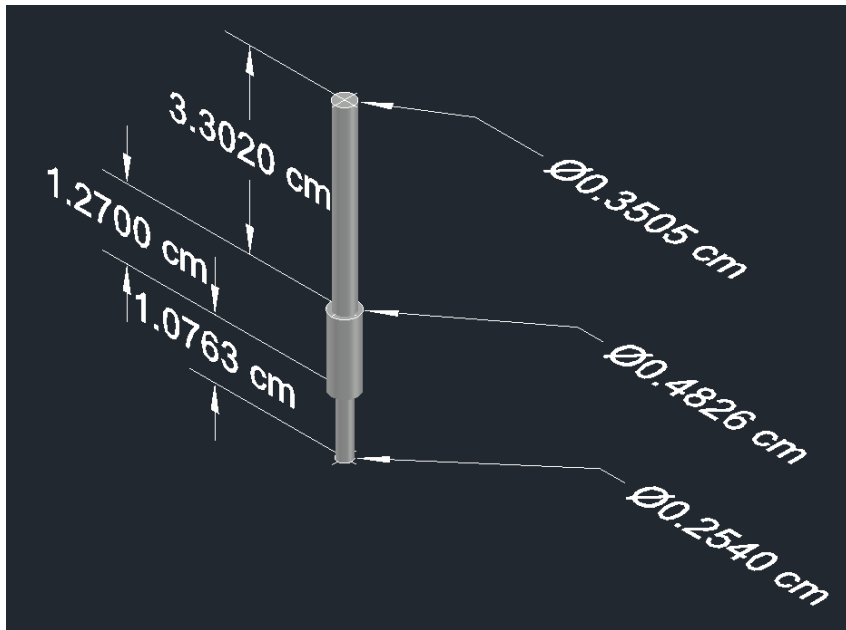


Figure 18. Schematic of steel rod. The upper portion of the rod is threaded to be a 6-32 screw, then the tungsten filaments are spot welded to the tip. The lower portion connects to the electrical feedthrough on which the evaporator is mounted.

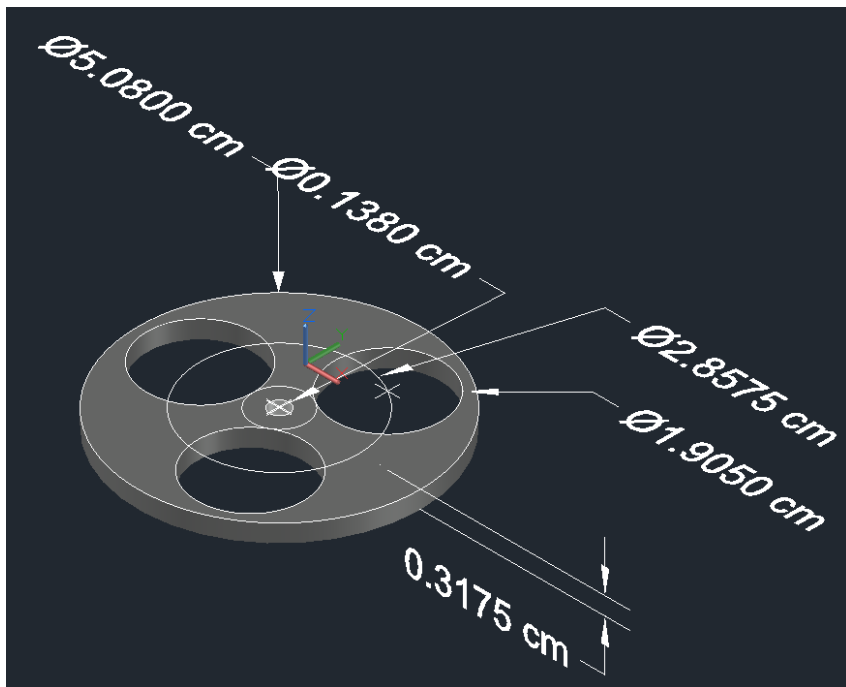


Figure 19. Schematic of tantalum crucible holder. Each of the three holes holds a graphite crucible.

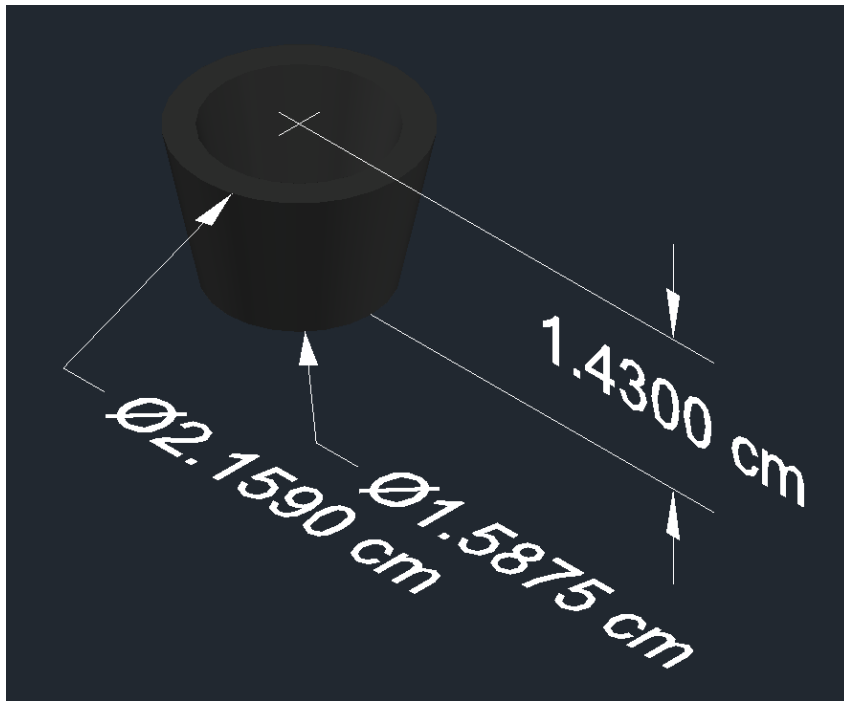


Figure 20. Schematic of graphite crucible. The crucible is a mostly hollow conical frustum.

3.3.3. Substrate Holder

The silicon substrate is affixed (see Figure 21) to a rotary feedthrough using an aluminum cylinder and disk. The substrate is affixed to the aluminum plate using steel paper clips and ceramic plates, and the paper clips are connected to the electrical feedthrough using tungsten wire. Under each paper clip is a layer of silver paint. An ohmmeter reads the resistance between the two paper clips. If no film has been deposited, the ohmmeter will read the high resistance of the silicon substrate. However, once a film has been deposited, the film will form a low resistance connection between the opposing paper clips.

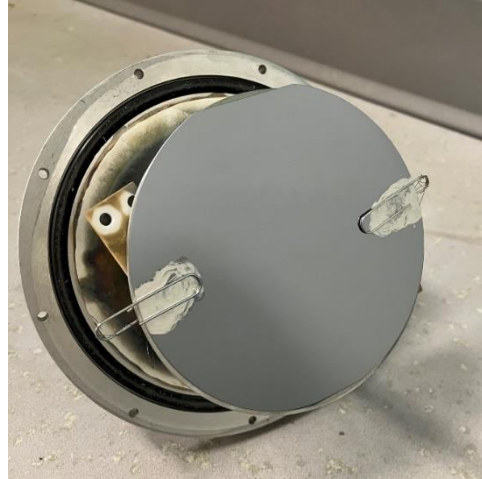


Figure 21. Images of substrate holder. Two pins of an electrical feedthrough are connected to metal paper clips resting on silver paint. An ohmmeter reads the resistance across the two pins, so when the film forms, a low resistance connection is formed, showing that a film has been created.

3.3.4. Deposition Rate Monitor

The deposition rate monitor used (Figure 22) is almost identical to the device used by Giedd and Perkins as described in section 1.3. The device collects evaporated material by evaluating the ionization rate and sends a current to an ammeter. This current can then be used to determine the rate of evaporation. The device is, as of yet, untested.

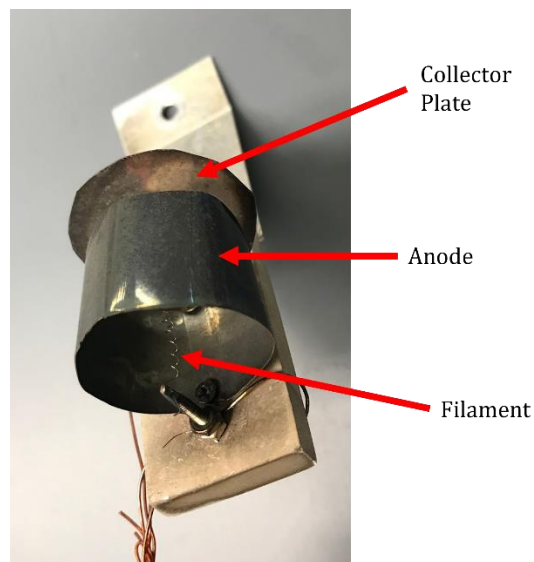


Figure 22. Image of deposition rate monitor. The filament supplies the ionizing electrons, the anode accelerates the ions, and the collector plate collects the ions and produces current based on the number of ions collected.

Chapter 4

EXPERIMENT AND RESULTS

With the installation of the new evaporator, it became necessary to evaluate the system's performance. First, the system was degassed. This was achieved by putting a constant voltage across the filament and slowly increasing the current to 3 A, not allowing the chamber pressure to surpass $3 \cdot 10^{-5}$ Torr. Following this procedure, a thin silver film was produced (

Figure 23) during a test of the evaporation system.

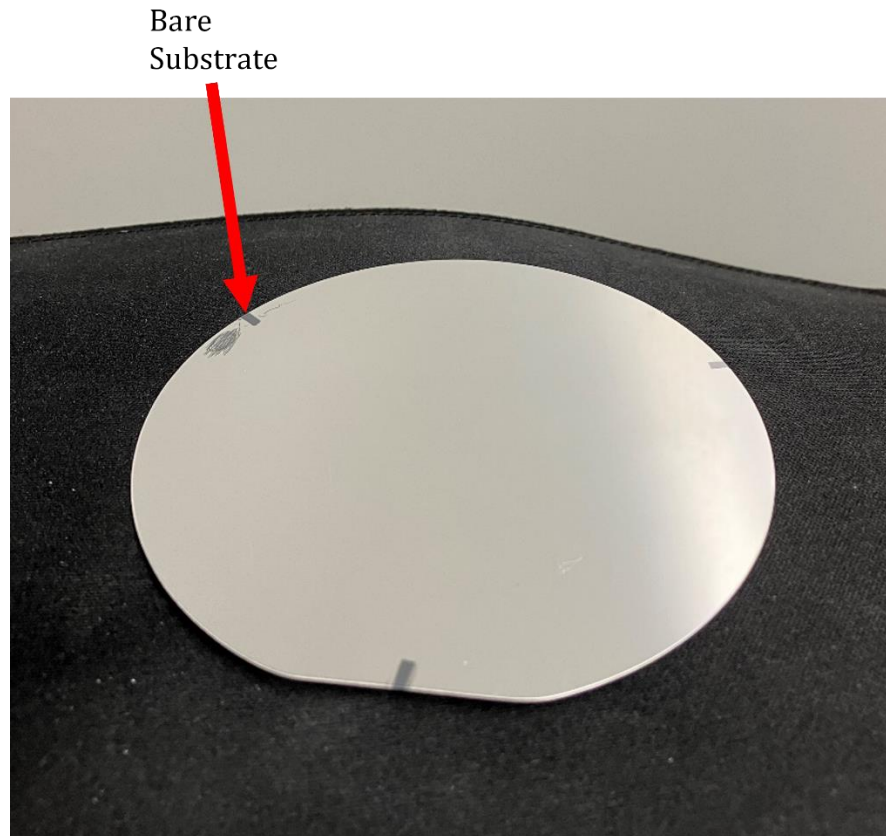


Figure 23. Image of Ag film on Si substrate. The bare substrate is where the previous holder contacted the substrate. The power used to create this film was approximately 300 W.

During the experiment, the filament current was 2.7 A, the potential difference between the filament and crucible had reached a peak of -1710 V AC, the peak thermionic current was approximately 240 mA and the peak thermionic power was approximately 410 W. The interior of the viewport located at the side of the chamber appeared to be coated in silver residue. After removing the substrate, a film had indeed been deposited, so another substrate was placed in the chamber. The film was made by melting and evaporating small cylindrical silver pellets with 99.99% purity. The weight of the substrate was not determined before being placed in the chamber, so several substrates were weighed to find the average weight of a substrate. The weight of the film was determined by weighing the film and substrate and comparing the weight to the weight of the average substrate. By using the density of silver and the area of the film, the deposited film was determined to have an average thickness of $14.99 \mu\text{m} \pm 3.08 \mu\text{m}$. The majority of this error came from averaging the weights of several substrates and can be eliminated by using the weight of the substrate placed in the chamber.

Chapter 5

STATE OF THE CHAMBER AND FUTURE WORK

The chamber is currently capable of producing films, but the process for creating said films is not ideal for a few main reasons. Firstly, the filament current is controlled by a variable coil resistor floating at high negative voltage, which means changing the resistance requires turning off the high voltage. Because of this, it is impossible to alter the current of the filament during the evaporating process. Secondly, the process of heating the filament can take several hours in some cases, as any oxidation must be baked off. With this process, heating up the filament increases the pressure of the chamber, and if the pressure gets too high, the filament can break. For this reason, the filament must be heated up slowly. A system is currently being conceived that could use an Arduino to turn up the high voltage to heat the filament but do this at a rate that would not cause the filament to break. This way, one individual would not have to sit and adjust the voltage slowly over several hours, watching the pressure the whole time. Thirdly, it would be ideal to know the deposition rate at a given time. For this, the evaporation rate monitor, mentioned in Section 3.3.4, must be calibrated to provide an accurate current that is related to the rate of evaporation and therefore deposition.

References

-
- [1] K. Priya *et al.*, IOP Conf. Ser.: Mater. Sci. Eng. **360** (2018).
- [2] K. Bordo, H. G. Rubahn, Mater. Sci. **18** (2012).
- [3] P. Wanarattikan, P. Jitthamapirom, R. Sakdanuphab, A. Sakulkalavek, Adv. Mater. Sci. Eng. **2019** (2019).
- [4] S. H. Lim, H. K. Kim, Sci. Rep. **10** (2020).
- [5] A. G. Emsile, F. T. Bonner, L. G. Peck, J. Appl. Phys. **29**, 858-862 (1958).
- [6] W. E. Sayer, A. Man, U.S. Patent No. 229335 (29 June 1880).
- [7] T. Suntola *et al.*, U.S. Patent No. 4058430 (15 November 1977).
- [8] W. R. Grove, Phil. Tran. R. Soc. London **142**, 87-101 (1852).
- [9] M. Faraday, Proc. R. Soc. London **8**, 356-361 (1857).
- [10] K. K. Rajesh *et al.*, Vacuum **141**, 230-234 (2017).
- [11] Eiji Makino, M. Uenoyama, T. Shibata, Sens. Actuator A Phys. **71**, 187-192 (1998).
- [12] M.F. Al-Kuhaili, E.E. Khawaja, D.C. Ingram, S.M.A. Durrani, Thin Solid Films **460**, 30-35 (2004).
- [13] K. Priya, V.K. Ashith, Gowrish K. Rao, Ganesh Sanjeev, Ceram. Int. **43**, 10487-10493 (2017).
- [14] Albert Folch, Javier Tejada, Christopher H. Peters, Mark S. Wrighton, Appl. Phys. Lett. **66**, 2080 (1995).
- [15] K. Goedicke, B. Scheffel, S. Schiller, Surf. Coat. Technol. **68-69**, 799-803 (1994).
- [16] J. R. Nicholls *et al.*, Corrosion Sci. **35**, 1209-1223 (1993).
- [17] L. I. Maissel, R. Glang (Eds.), *Handbook of Thin Film Technology*, McGraw-Hill p. 1-26 - 1-36, 1-90 (1970).
- [18] H. M. O'Bryan, Rev. Sci. Instrum. **5** 125 (1934).
- [19] Neelam *et al.*, Vacuum **170** (2019).
- [20] G. Sauerbrey, Zeitschrift für Physik **155**, 206-222 (1959).
- [21] G. R. Giedd, M. H. Perkins, Rev. Sci. Instrum. **31**, 773-775 (1960).
- [22] O. v. Guericke, M. G. F. Ames, *The New (So-Called) Magdeburg Experiments of Otto Von Guericke* (1994).
- [23] R. Boyle, *New Experiments Physio-Mechanicall Touching the Air* (1660).
- [24] <https://www.beautifulchemistry.net/boyle>
- [25] H. Sprengel, J. Chem. Soc. London **18**, 9-21 (1865).
- [26] C. C. Barnes, CA. Patent No. 3559 (15 June 1874).
- [27] W. Becker, Vacuum **16**, 625-632 (1966).
- [28] L. D. Hall, J. C. Helmer, R. L. Jepsen, U.S. Patent No. 2993638 (25 July 1961).
- [29] P. Strubin, J. Vac. Sci. Technol. **17** (1979).
- [30] M. Kirkland, B.S. Thesis, Houghton College (2016).
- [31] S. Daigler, B.S. Thesis, Houghton College (2015).
- [32] J. Wilson, B.S. Thesis, Houghton College (2023).
- [33] O. W. Richardson, "Thermionic phenomena and the laws which govern them" Nob
- [34] J. R. Rumble (Ed.), *Handbook of Chemistry and Physics 103rd Edition* (2022)
- [35] A. Redman, B.S. Thesis, Houghton College (2017).